Single- and Two-Stage Inverter-Based Grid-Connected Photovoltaic Power Plants With Ride-Through Capability Under Grid Faults

Mitra Mirhosseini, *Student Member, IEEE*, Josep Pou, *Senior Member, IEEE*, and Vassilios G. Agelidis, *Senior Member, IEEE*

***Abstract*—Grid-connected distributed generation sources interfaced with voltage source inverters (VSIs) need to be disconnected from the grid under: 1) excessive dc-link voltage; 2) excessive ac currents; and 3) loss of grid-voltage synchronization. In this paper, the control of single- and two-stage grid-connected VSIs in photovoltaic (PV) power plants is developed to address the issue of inverter disconnecting under various grid faults. Inverter control incorporates reactive power support in the case of voltage sags based on the grid codes' (GCs) requirements to ride-through the faults and support the grid voltages. A case study of a 1-MW system simulated in MATLAB/Simulink software is used to illustrate the proposed control. Problems that may occur during grid faults along with associated remedies are discussed. The results presented illustrate the capability of the system to ride-through different types of grid faults.**

***Index Terms*—DC–DC converter, fault-ride-through, photovoltaic (PV) systems, power system faults, reactive power support.**

I. Introduction

FAULT STUDIES are important in large-scale grid-connected renewable energy systems and have been reported in the technical literature. However, most of these studies focused on grid-connected wind power plants [1], [2]. In the case of grid-connected photovoltaic (PV) power plants (GCPPPs), research reported thus far focused on fault-ride-through (FRT) capability [3], [4]. Specifically, a three-phase current-source inverter (CSI) configuration was investigated under various fault conditions in [5] and [6], in which the output currents remain limited under all types of faults due to the implementation of a current-source model for the inverter. However, this configuration may lead to instability under dynamic conditions [7]. Three-phase voltage source inverters (VSIs) are used in grid-connected power conversion systems. Due to the increasing number of these systems, the control of the VSIs is required to operate and support the grid based on the grid codes (GCs) during voltage disturbances and unbalanced conditions.

Among several studies for unbalanced voltage sags, a method was introduced in [8] to mitigate the peak output currents of a 4.5-kVA PV system in nonfaulty phases. Another study in [9] presented a proportional-resonant (PR) current controller for the current limiter to ensure sinusoidal output current waveforms and avoid over-current. However, in the mentioned studies, reactive power support was not considered. In [10], a study dealing with the control of the positive and negative sequences was performed. Two parallel controllers were implemented, one for each sequence. The study demonstrated the dynamic limitations of using this control configuration due to the delays produced in the current control loops. A study was reported in [11] for the control of the dc side of the inverter, which shows the impact of various types of faults on the voltage and current of the PV array.

Considering FRT strategies for grid-connected VSIs, some research has been done on wind turbine applications [12]–[14] and also on VSI-based high-voltage direct current (HVDC) systems [15]–[17]. Some of these studies are based on passive control, e.g., crowbar and chopper resistors [14], [15], whereas others are based on active control schemes [12], [13], [16], [17]. Although both categories can provide FRT capability, the passive methods have the drawbacks of requiring additional components and dissipating significant power during the voltage sag processes. In the application of GCPPPs with the configurations of single-stage conversion (single-stage conversion means direct connection of the PV source to the dc side of the VSI), some research were done in [18] and [19] evaluating the FRT issues of both ac and dc sides of the inverter under unbalanced voltage conditions. However, in the application of a two-stage conversion (meaning a dc–dc conversion or preregulator unit exists between the PV source and VSI), no paper so far has proposed a comprehensive strategy to protect the inverter during voltage sags while providing reactive power support to the grid. All the designs and modifications for the inverter in both the single- and two-stage conversions have to accommodate various types of faults and address FRT capability based on the GCs [20]. PV inverter disconnection under grid faults occurs due to mainly three factors: 1) excessive dc-link voltage; 2) excessive ac currents; and 3) loss of grid voltage synchronization, which may conflict with the FRT capability.

Manuscript received December 09, 2013; revised April 11, 2014 and May 26, 2014; accepted July 17, 2014.

M. Mirhosseini and V. G. Agelidis are with the Australian Energy Research Institute (AERI), School of Electrical Engineering and Telecommunications, University of New South Wales (UNSW), Sydney, NSW 2052, Australia (e-mail: m.mirhosseini@student.unsw.edu.au; vassilios.agelidis@unsw.edu.au).

J. Pou is with the Australian Energy Research Institute (AERI), School of Electrical Engineering and Telecommunications, University of New South Wales (UNSW), Sydney, NSW 2052, Australia, on leave from the Technical University of Catalonia, 08222 Terrassa, Spain (e-mail: j.pou@unsw.edu.au; josep.pou@upc.edu).

Color versions of one or more of the figures in this paper are available online at http://ieeexplore.ieee.org.

Digital Object Identifier 10.1109/TSTE.2014.2347044

In this paper, the control strategy introduced in [18] for a single-stage conversion is used, although the voltage sag detection and reactive power control is modified based on individual measurements of the grid voltages. The main objective of this paper is to introduce new control strategies for the two-stage conversion in GCPPPs that allow the inverter to remain connected to the grid under various types of faults while injecting reactive power to meet the required GCs. Some selected simulation results for single- and two-stage configurations are presented to confirm the effectiveness of the proposed control strategies.

This paper is organized as follows. A brief introduction to the GCs for GCPPPs connected in the medium-voltage (MV) grids is presented in Section II. A case study for single-stage VSI-based GCPPPs is introduced in Section III. The same section includes discussions on the implemented grid synchronization method as well as the control strategy to avoid excessive ac currents and excessive dc voltage under voltage sags. In the case of two-stage VSI-based GCPPPs, a case study of 1-MVA system is presented in Section IV and three remedies are proposed to ride-through different types of faults and solar radiation conditions. Finally, Section V summarizes the conclusion of this paper.

II. Grid Codes

As the German GCs are the most comprehensive codes for the different power levels of PV installations and integration technologies [21], this paper follows these codes as a basis for the discussions. During voltage sags, the GCPPP should support the grid voltage by injecting reactive current. The amount of reactive current is determined based on the droop control defined as follows:

$$i_{q\text{ref}} = \text{droop}\,|\text{d}e_L|\,I_n \quad \text{for} \quad \frac{|\text{d}e_L|}{E_n} \geq 10\% \quad \text{and} \quad \text{droop} \geq 2 \tag{1}$$

where droop is a constant value, $\text{d}e_L$ is the amount of voltage drop, and I_n is the rated current of the PV inverter in *dq* coordinates, i.e., $I_n = \sqrt{3}I_n$, where I_n is the rated rms line current of the inverter. The amount of voltage drop $\text{d}e_L$ is obtained based on the lowest rms value of the line-to-line voltages of the three phases at the terminal of the GCPPP, i.e., $e_{L\,\min}$ shown in Fig. 1. The rms voltage is obtained using the following expression:

$$e_{L\text{rms}} = \sqrt{\frac{1}{T_w}\int_{t-T_w}^{t} e_L{}^2\,\text{d}t}, \quad \text{with } T_w = \frac{T}{2} \tag{2}$$

where e_L is the instantaneous line-to-line voltage, T_w is the window width for the rms value calculation, and T is the grid voltage period, which is equal to 20 ms for a grid frequency of 50 Hz. The resulting control diagram for the reactive current generation is depicted in Fig. 1.

III. Case Study For a Single-Stage Conversion

In this section, a 1-MVA single-stage GCPPP is considered. It is modeled using MATLAB/Simulink and the system main specifications are summarized in Table I from the data given in [22] and [23]. Fig. 2 shows the model of the GCPPP. In [24], concerning the FRT capability, the inverter disconnection factors are illustrated according to the GCs [21].

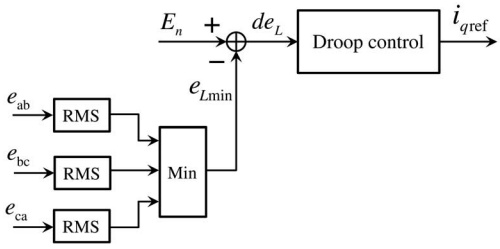

Fig. 1. Droop control diagram for the reactive current reference provision.

TABLE I
Case Study System Specifications

PV module specifications		PV inverter specifications	
Maximum operating voltage (V_{mpp})	35.6 V	Maximum dc power	1133 kW
Maximum operating current (I_{mpp})	8.29 A	Maximum dc input voltage	1000 V
Open circuit voltage (V_{oc})	44.3 V	Rated dc voltage	800 V
Short circuit current (I_{sc})	8.74 A	Apparent power rating (at STC)	1100 kVA
Number of parallel modules, n_p	155	**Filter**	R = 1 mΩ L = 150 μH
Number of series modules, n_s	22	**Transformer**	1.2 MVA 20/0.415 kV Dyn11 50 Hz

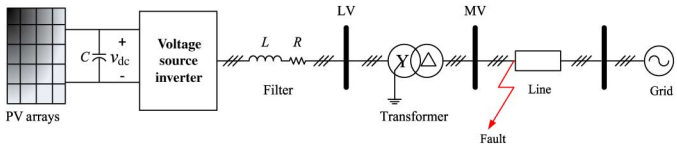

Fig. 2. Diagram of a single-stage GCPPP.

A. Grid Voltage Synchronization

In grid-connected inverters, one important issue is the voltage phase angle detection. This is usually performed by phase-locked-loop (PLL) technique based on a synchronous reference frame PLL (SRF-PLL) [25], known as conventional PLL. The conventional PLL configuration does not perform well under unbalanced voltage sags and consequently may lead to the inverter being disconnected from the grid [24].

Several methods were proposed to extract the voltage phases accurately under unbalanced voltage conditions [26]–[29]. In this paper, the method based on moving average filters (MAFs) introduced in [28] is applied, which was also used in [24] showing very satisfactory performance. In this method, the positive sequence of the voltage is extracted from the grid by means of an ideal low-pass filter. Then, the angle of the positive sequence is detected.

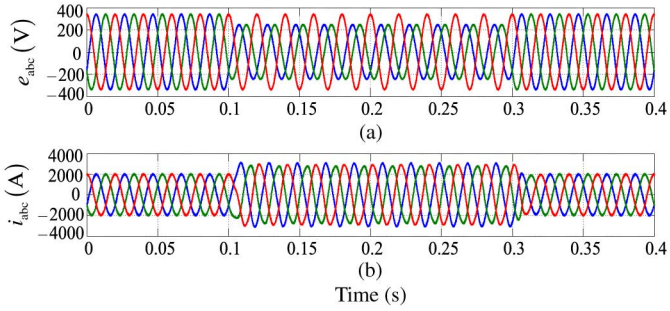

Fig. 3. (a) Grid voltages and (b) grid currents at the LV side under 60% SLG voltage sag produced at MV side of the transformer.

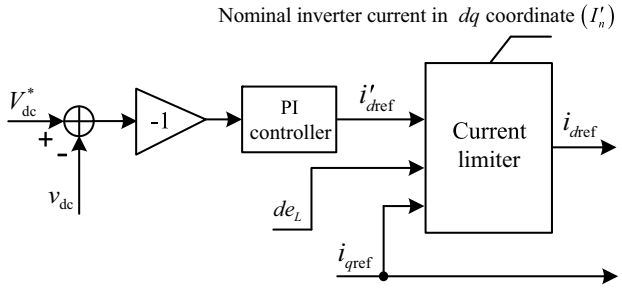

Fig. 4. Control diagram of the current limiter.

B. Excessive AC Current

Commercial grid-connected inverters have a maximum ac current value specified. If any of the currents exceed such value, the inverter is disconnected from the grid. Under a grid voltage sag, the d-component of the current (in the SRF) increases because the controller wants to maintain the active power injected into the grid and grid voltages are temporarily reduced. In addition to the increase of the d current component, the inverter has to inject reactive current during the fault to meet the FRT requirements. The amount of reactive current is assigned according to the droop control given in (1). Since the d and q current components increase, this may lead the over-current protection to disconnect the inverter from the grid.

In this case study, according to the specifications of the PV modules and their numbers of being connected in series and parallel given in Table I, the maximum power injected under standard test conditions (STC) is 1.006 MW. This power gives a rated rms current value of 1399.5 A (a peak value of 1979 A) at the low-voltage (LV) side of the transformer considering 100% efficiency for the GCPPP. According to the the inverter datasheets, the maximum acceptable output current at the LV side of the transformer is 1532 A (a peak value of 2167 A). In the case of a fault, e.g., a single-line-to-ground (SLG) voltage sag at the MV side of the transformer as the one presented in Fig. 3, the output currents exceed the limits. This will lead to inverter disconnection, although it is not applied in this simulation. Unbalanced and distorted currents are produced because the instantaneous output power and the dc-link voltage have low-frequency ripples, and therefore, the active current reference contains low-frequency ripples as well. The final reference for the d current component (i_{dref}) should be limited considering the need of reactive current injection as shown in Fig. 4. It

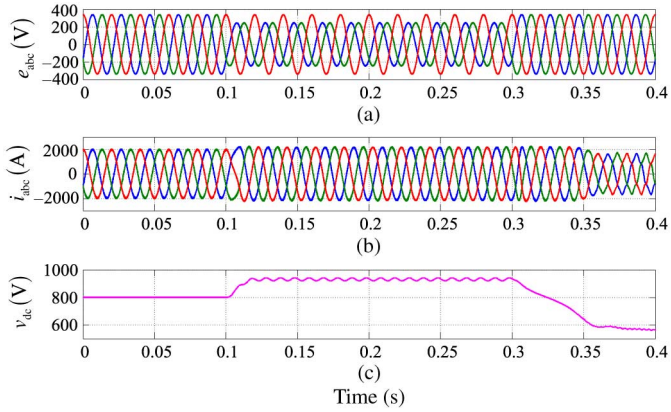

Fig. 5. Adding the current limiter to the VSI control: (a) grid voltages; (b) grid currents; and (c) dc-link voltage under an SLG-voltage sag at MV side of the transformer.

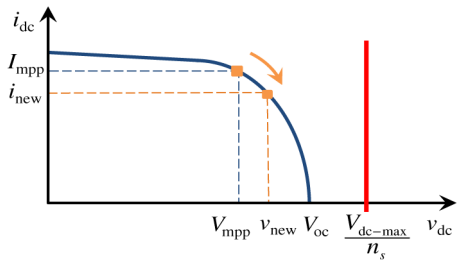

Fig. 6. Change in the PV operating point under voltage sag and maximum acceptable dc-link voltage.

should be mentioned that all the voltage sag case studies in this paper are applied to the MV side for the time period $t = 0.1$ s to $t = 0.3$ s, whereas the resultant ac voltages and currents shown in the figures are presented with their equivalent magnitudes at the LV side.

Fig. 5 shows the generated currents after applying the current limiter in this example. One can observe in Fig. 5(b) that the grid currents are balanced. This is because the active current reference (i_{dref}) is limited to an almost constant value during the voltage sag. It should be mentioned that when operating with low solar radiation and/or small voltage sags, the active current reference may not be limited and therefore, it goes through the current limiter without being affected, i.e., $i_{dref} = i_{dref}$. As a consequence, if the voltage sag was unbalanced, the active current reference and consequently the output currents would contain some low-frequency harmonics.

C. Excessive DC-Link Voltage

If the active current reference is limited, i.e., $i_{dref} < i_{dref}$, the generated power from the PVs is more than the injected power into the electrical grid. As a consequence, some energy is initially accumulated into the dc-link capacitor, increasing the dc bus voltage as shown in Fig. 5(c). In a single-stage GCPPP, as the dc-link voltage increases, the operating point on the $I-V$ curve of PV array moves toward the open-circuit voltage point (V_{oc}), which leads the PV current to decrease, as shown in Fig. 6. The power generated by the PV panels

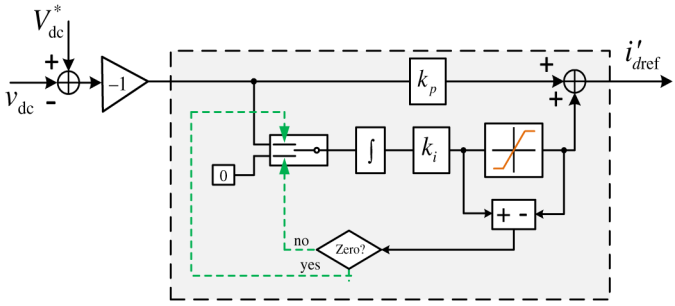

Fig. 7. PI controller with an anti-wind-up technique.

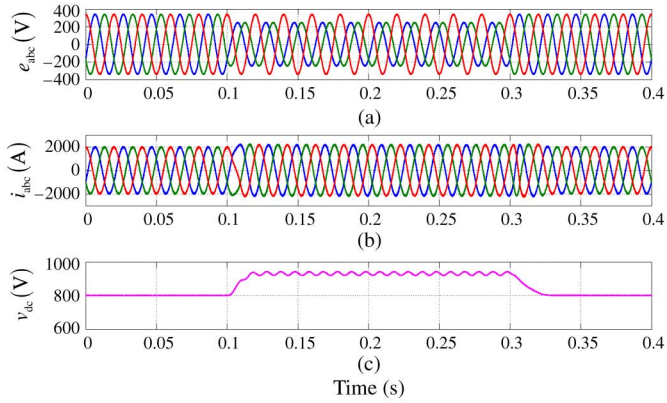

Fig. 8. Application of an anti-wind-up technique to the PI controller: (a) grid voltages; (b) grid currents; and (c) dc-link voltage under 60% SLG voltage sag at MV side of the transformer.

is reduced because the operating point is taken away from the maximum power point (MPP) and therefore, less active current is injected into the ac side. This happens until the GCPPP reaches a new steady state where the dc-link voltage stops increasing. Thus, single-stage GCPPPs are self-protected because the generated power is reduced when the dc-link voltage increases under ac faults. It should be mentioned that the inverter has to withstand the worst case of the dc-link voltage, which is produced when the voltage provided by the PV modules reaches the open-circuit value (V_{oc}) under the maximum solar radiation expected on the generation site. Hence, the number of PV modules connected in series (n_s) has to be limited in the design of the GCPPPs so that the dc-link voltage is never higher than the maximum acceptable value of the inverter (V_{dc-max})

$$n_s \leq \frac{V_{dc-max}}{V_{oc}}. \tag{3}$$

Fig. 6 shows this concept in the case of a single-stage GCPPP. A problem that may appear because of the deviation of the MPP during the voltage sag is that, after the fault being cleared, the dc-link voltage and ac currents may take a long time to reach the prefault values, as shown in Fig. 5(b) and (c). The reason is that the error in the dc-link voltage produces accumulation of control action to the integral part of the proportional-integral (PI) controller (Fig. 4). This control action is limited by the current limiter and thus it has no effect on the grid currents. However, when the voltage sag ends, the excessive control action accumulated in the integral part of the controller has to be compensated by an input error in the opposite direction. As a consequence, the dc-link voltage is reduced below the reference value. In this case, a significant decrease of the dc-link voltage may lead to inverter losing control and be disconnected. To overcome this issue, an anti-wind-up technique is applied to stop the PI controller accumulating excessive control action when it exceeds a specified value [30]. The schematic of the anti-wind-up technique is shown in Fig. 7 in which V_{dc} and v_{dc} are the reference and actual dc-link voltages, respectively. The improved results when applying the anti-wind-up technique are depicted in Fig. 8. In this case, once the grid fault is cleared, the dc-link voltage recovers to the prefault value with no perceptible overcompensation.

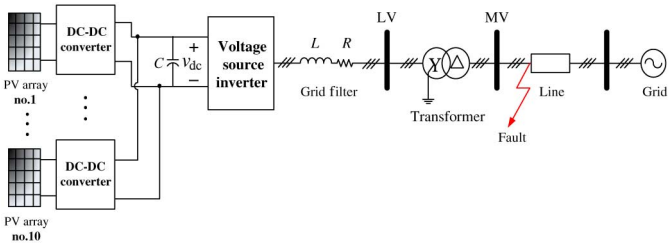

Fig. 9. Diagram of the two-stage conversion-based GCPPP.

IV. Case Study For a Two-Stage Conversion

A two-stage GCPPP includes a dc–dc converter between the PV arrays and the inverter. In high-power GCPPPs, more than one dc–dc converter can be included, one per each PV array. Despite having several dc–dc converters, these systems will be referred anyway as two-stage GCPPPs. In two-stage GCPPPs, the MPP tracking (MPPT) is performed by the dc–dc converter and the dc-link voltage is regulated by the inverter.

During a voltage sag, if no action is taken in the control of the dc–dc converter, the power from the PV modules is not reduced and therefore, the dc-link voltage keeps rising and may exceed the maximum limit. Hence, the system is not self-protected during grid fault conditions. A specific control action has to be taken to reduce the power generated by the PV modules and provide the two-stage GCPPP with FRT capability.

A simple method to provide dc-link overvoltage protectioni consists on shutting down the dc–dc converter when the dc voltage rises above a certain limit. The dc–dc converter can be reactivated when the dc-link voltage is below a certain value using a hysteresis controller. In the solutions proposed in this paper, the dc-link voltage is controlled during the voltage sag process and there is no significant increase in the dc-link voltage during this transient.

The diagram of the case study for a two-stage GCPPP is shown in Fig. 9. It consists of a 1-MVA inverter and 10 parallel 100-kW dc–dc boost converters. Details of the individual dc–dc converter as well as the PV array characteristics connected to each dc–dc converter are summarized in Table II. The rest of data for this system are provided in Table I.

TABLE II
PV ARRAYS AND DC–DC CONVERTER SPECIFICATIONS IN TWO-STAGE GCPPP

DC–DC converter and PV array specifications			
Input voltage of the dc–dc converter at MPP, V_{PV}	356 V	Output voltage of the dc–dc converter, V_{dc}	800 V
Number of parallel PV modules in each array, n_p	34	DC–DC converter inductance, L_i	1 mH
Number of series PV modules in each array, n_s	10	DC-link capacitance, C	31 mF

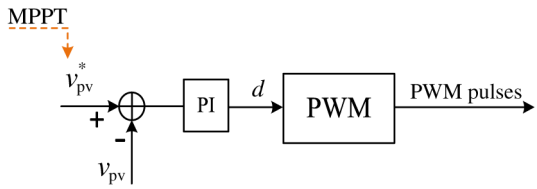

Fig. 10. Control diagram of the dc–dc converter.

In two-stage GCPPPs, the PV voltage (v_{pv}) is controlled by the duty cycle (d) of the dc–dc converter. The reference for the PV voltage is given by the MPPT, as shown in Fig. 10.

A feed-forward strategy is applied to improve the dynamics of the dc-link voltage. The strategy is based on the assumption that the PV generated power is equal to the injected power into the grid, i.e.,

$$i_{\text{pv}} v_{\text{pv}} = e_d i_d + e_q i_q \tag{4}$$

where i_{pv} and v_{pv} are the PV current and voltage, respectively, and e_d and e_q are the d and q grid voltage components extracted by the PLL. Since the PLL forces the e_q component to be zero, the estimated d current component is obtained as

$$i_{d-\text{est}} = \frac{i_{\text{pv}} v_{\text{pv}}}{e_d}. \tag{5}$$

In two-stage GCPPPs, three different ways to limit the dc-link voltage under fault conditions are proposed: 1) short-circuiting the PV array by turning ON the switch of the dc–dc converter throughout the voltage sag duration; 2) leaving the PV array open by turning OFF the switch of the dc–dc converter; and 3) changing the control of the dc–dc converter to inject less power from the PV arrays when compared with the prefault operating conditions.

It should be mentioned that in all the configurations including single-stage conversion, the MPPT is disabled during the voltage sag condition and the voltage reference of prefault condition (V_{mpp}) is considered. Once the fault ends, the MPPT is reactivated. In the two-stage topology, the first two solutions explained next stop transferring energy from the PV arrays to the dc bus, whereas the dc bus keeps regulated at the reference value by the voltage control loop. In the third method, the MPPT is disconnected and the PV operating point moves to a lower power level to avoid overvoltage in the dc-link. Therefore, no matter the MPPT technique is voltage or current controlled and the algorithms implemented for the MPPT, the performance of the proposed methods during the voltage sag condition remains the same because the MPPT is disconnected during the voltage sag.

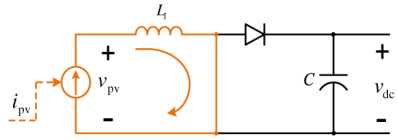

Fig. 11. Current path when short-circuiting the PV panels.

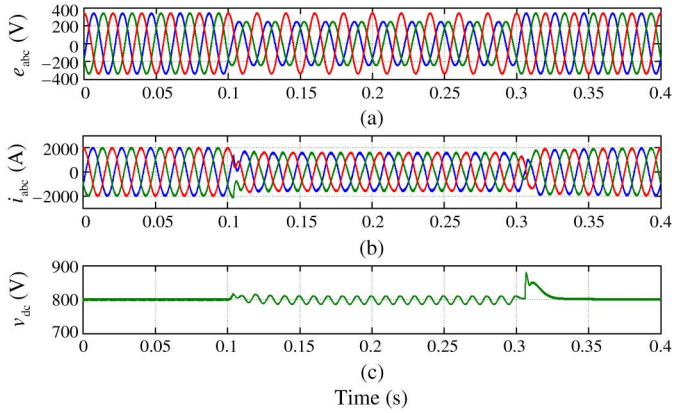

Fig. 12. Short-circuiting the PV panels: (a) grid voltages; (b) grid currents; and (c) dc-link voltage when applying a 60% SLG voltage sag at MV side of the transformer.

A. Short-Circuiting the PV Panels

In this method, the dc–dc converter switch is ON ($d = 1$) throughout the voltage sag, as shown in Fig. 11. Consequently, no power is transferred from the PV modules to the dc-link. Since v_{pv} is zero, the feed-forward term $i_{d-\text{est}}$ in (5) defines a fast transition to zero at the beginning of the voltage sag, accelerating the overall dynamic of the controller. Fig. 12 shows some results for an SLG voltage sag with a 60% voltage drop at MV side occurred from $t = 0.1$ s to $t = 0.3$ s. The generated power of the PV arrays and also the injected active and reactive power into the grid are shown in Fig. 13. During the voltage sag, the dc-link voltage remains relatively constant, $i_{d\text{ref}}$ becomes almost zero with some ripples, and only $i_{q\text{ref}}$ is injected during the fault period. Consequently, the current limiter does not have to be activated in this case. Under unbalanced voltage sags, the output power contains a second-order harmonic [31], which will produce dc-link voltage ripples at the same frequency.

B. Opening the Circuit of the PV Panels

Another option to avoid transferring power from the PV modules to the dc-link is to keep the dc–dc converter switch OFF throughout the voltage sag ($d = 0$), as shown in Fig. 14. Since, the inverter is not transferring active power into the grid during the voltage sag, the PV voltage v_{pv} increases until the dc–dc converter inductor is completely discharged ($i_{\text{pv}} = 0$). Then, the diode turns OFF and the PV modules stop providing energy into the dc-link [Fig. 14(b)]. This case is similar

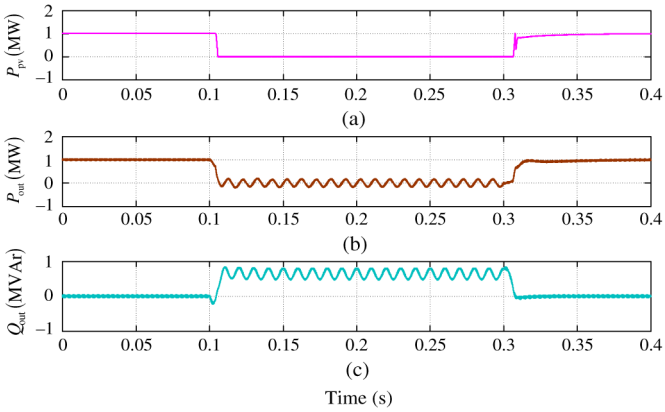

Fig. 13. Short-circuiting the PV panels: (a) overall generated power; (b) injected active power; and (c) reactive power to the grid.

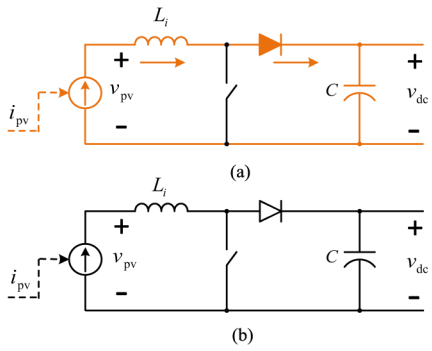

Fig. 14. Current paths in dc–dc converter when turning ON the switch: (a) transition mode and (b) locked in state.

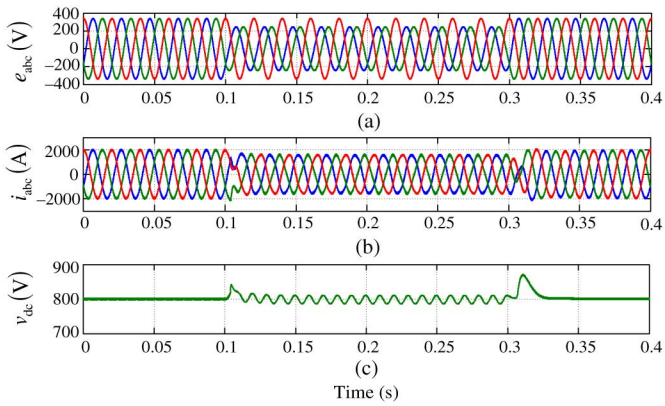

Fig. 15. Turning the dc–dc converter switch ON: (a) grid voltages; (b) grid currents; and (c) dc-link voltage when applying a 60% SLG voltage sag at the MV side.

to the previous one where the diode was continuously ON and no current from the PV was provided to the dc-link. The main difference with the previous case is the transition process, as depicted in Fig. 15.

C. Injecting Less Power From the PV Panels

In the two previous cases, during the voltage sags, there is no power generated by the PV panels and therefore, only reactive current is injected into the grid. However, as mentioned in [21],

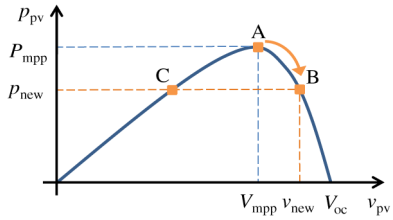

Fig. 16. $P-V$ curve and new power point under voltage sags.

the network operator is allowed to feed the grid through the generating power plant during the voltage sags. For this purpose, the GCPPP is controlled to inject less power into the grid during the voltage sag compared with the prefault case, while avoiding overvoltage in the dc-link.

In normal operation, the MPPT function is performed by the dc–dc converter, whereas the dc-link voltage is regulated by the inverter. However, under a voltage sag, some modifications should be implemented in order to keep the GCPPP grid-connected. The proposed method tries to match the power generated by the PV modules with the power injected into the grid while trying to keep the dc-link voltage constant. Unlike the previous cases of keeping the switch ON or OFF during the voltage sag, in this case, power balance is achieved for a value different from zero. Therefore, both active and reactive currents will be injected into the grid.

In the proposed method, the target of the dc–dc converter is no longer achieving MPP operation but regulating the power generated by the PVs to match the maximum active power that can be injected into the grid. The dc–dc converter is controlled to find a proper value for the PV voltage (v_{pv}) that achieves such power balance. As a result, the operating point should move from point A in Fig. 16 to a lower power point, e.g., either the points B or C. In this paper, moving the operating point in the direction from A to B is applied and analyzed. For this purpose, a positive voltage value Δv_{pv} should be added to the V_{mpp} value that was on hold from the prefault situation, as follows:

$$v_{new} = V_{mpp} + \Delta v_{pv}. \tag{6}$$

This displacement of the operating point Δv_{pv} is achieved by means of a PI controller that regulates the dc-link voltage to the rated value. In order to achieve a faster dynamic, the energy in the dc-link capacitor ($\frac{1}{2}Cv_{dc}^2$) is regulated instead of the dc-link voltage (v_{dc}). The schematic of this controller is shown in Fig. 17 in which the limiter is used to ensure only positive values for Δv_{pv} in order to force the PV voltage to increase (move to the right-side of the MPP, i.e., from A to B in Fig. 16). It should be mentioned that Δv_{pv} is added to the prefault value only under voltage sags and it is disconnected during normal operation of the GCPPP.

To ensure a fast dynamic response and maintaining the stability of the GCPPP, a feed-forward control strategy is proposed and applied to the dc-link control loop. For this purpose, a linear estimation is made based on the $P-V$ curve shown in Fig. 16. Let us suppose the triangle represented by the vertices (P_{mpp}, V_{mpp}), (0, V_{mpp}), and (0, V_{oc}), as depicted in Fig. 18.

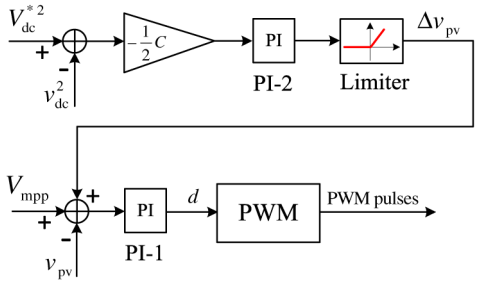

Fig. 17. Adding a controller to the dc–dc converter to force the operating point to move from the MPP to a lower power point.

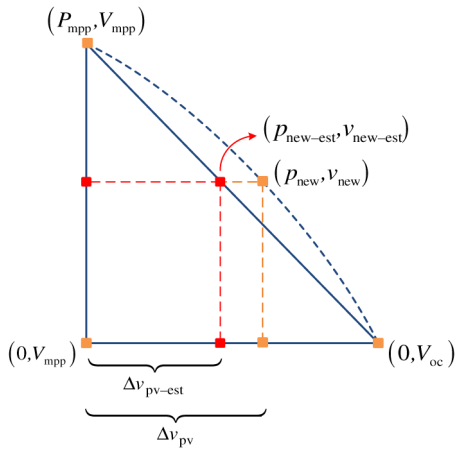

Fig. 18. Triangle used to estimate the new operating point.

The new point ($p_{\rm new}$, $v_{\rm new}$) can be estimated by ($p_{\rm new-est}$, $v_{\rm new-est}$) on the triangle hypotenuse. According to the Side-Splitter theorem and using interpolation, the estimation of $v_{\rm new-est}$ is

$$v_{\rm new-est} = \frac{p_{\rm new-est}}{P_{\rm mpp}}(V_{\rm mpp} - V_{\rm oc}) + V_{\rm oc} \tag{7}$$

in which $P_{\rm mpp}$ and $V_{\rm mpp}$ represent the prefault values at the MPP. The $p_{\rm new-est}$ can be calculated from the power injected into the grid

$$p_{\rm new-est} \simeq p_{\rm out} = e_d i_{d\rm ref}. \tag{8}$$

Substituting (8) into (7)

$$v_{\rm new-est} = \frac{e_d i_{d\rm ref}}{P_{\rm mpp}}(V_{\rm mpp} - V_{\rm oc}) + V_{\rm oc} \tag{9}$$

and

$$\Delta v_{\rm pv-est} = v_{\rm new-est} - V_{\rm mpp}. \tag{10}$$

The value in (10) is added to the controller as a feed-forward term before the limiter in Fig. 17, as shown in Fig. 19. In order to enhance the dynamics of the proposed controller further, another estimation can be derived using (9), which is the estimation of the duty cycle as a feed-forward term, $d_{\rm est}$. Based on

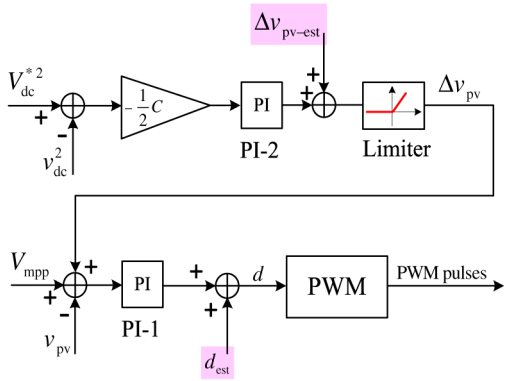

Fig. 19. Updated controller with feed-forward terms to enhance the dynamics of the proposed controller.

the relationship between the input and the output voltage of the boost dc–dc converter under continuous conduction operating conditions

$$\frac{v_{\rm dc}}{v_{\rm pv}} = \frac{1}{1-d} \tag{11}$$

the estimated duty cycle is

$$d_{\rm est} = 1 - \frac{v_{\rm new-est}}{V_{\rm dc}}. \tag{12}$$

The updated version of the controller in Fig. 17 is illustrated in Fig. 19, which contains the two feed-forward terms to enhance the dynamics of the proposed controller. The PI controllers PI-1 and PI-2 compensate for the difference between the estimated and the real values of d and $\Delta v_{\rm pv}$, respectively.

The only unknown variable in (9) is $i_{d\rm ref}$. The reason is that in the proposed method, during the voltage sag, the dc-link control loop stops adjusting the active current reference and instead regulates the input voltage of the dc–dc converter ($v_{\rm pv}$). The method proposed in this paper to estimate $i_{d\rm ref}$ is the following. Considering Fig. 4, the maximum value for the $i_{d\rm ref}$ is $i_{d\rm ref}$. Depending on the voltage sag depth and solar radiation (G), the value of $i_{d\rm ref}$ can be lower or equal to $i_{d\rm ref}$. Therefore, if the active current reference $i_{d\rm ref}$ can be estimated, $i_{d\rm ref}$ can be obtained as well. If $P_{\rm in}$ is the power generated by the PV array

$$P_{\rm in} \simeq e_d i_{d\rm ref} + e_q i_{q\rm ref} \tag{13}$$

and since e_q is zero, the estimated active current reference is

$$i_{d\rm ref-est} = \frac{P_{\rm in}}{e_d}. \tag{14}$$

The maximum acceptable value for the $i_{d\rm ref}$ can be obtained based on the prefault value of $P_{\rm in}$, i.e., $P_{\rm mpp}$ and e_d, as follows:

$$i_{d\rm ref-est} = \frac{P_{\rm mpp}}{e_d}. \tag{15}$$

The estimated current $i_{d\rm ref-est}$ goes through the current limiter and based on the required reactive current reference, $i_{d\rm ref}$

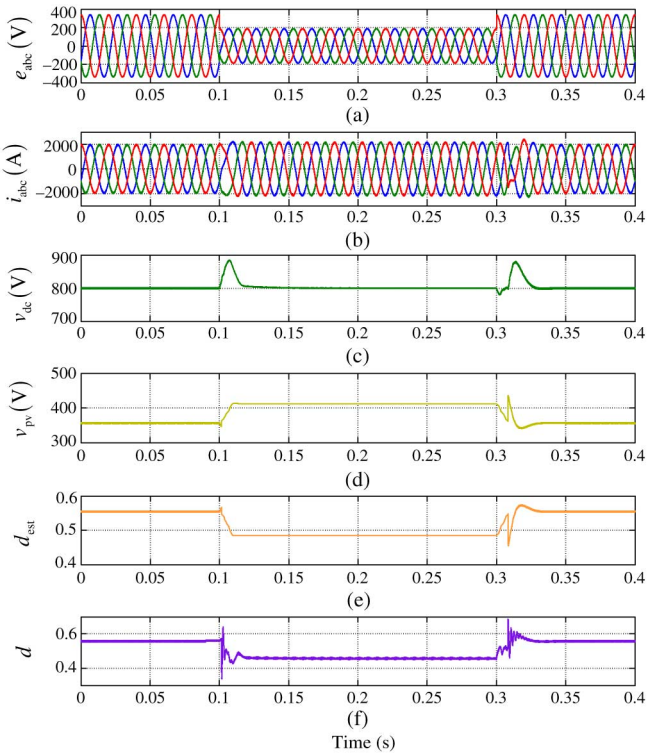

Fig. 20. Control of the dc–dc converter to produce less power under voltage sag: (a) grid voltages; (b) grid currents; (c) dc-link voltage; (d) input voltage of the dc–dc converter; (e) estimated duty cycle; and (f) actual duty cycle under a 3LG with 45% voltage sag at MV side.

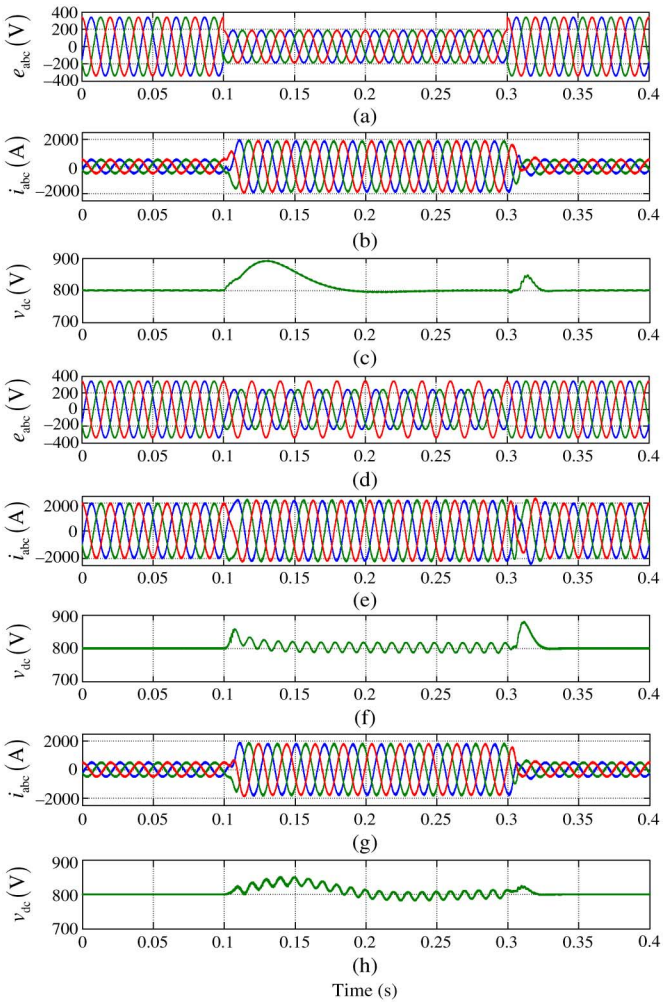

Fig. 21. Control of the dc–dc converter to produce less power under voltage sag: (a) grid voltages under a 3LG with 45% voltage sag at MV side; (b) related grid currents for $G = 300\,\mathrm{W/m^2}$; and (c) related dc-link voltage; (d) grid voltages under an SLG with 65% voltage sag at the MV side; (e) related grid currents for $G = 1000\,\mathrm{W/m^2}$; (f) related dc-link voltage; (g) related grid currents under $G = 300\,\mathrm{W/m^2}$; and (h) related dc-link voltage."

can be obtained and substituted in (9). The performance of the proposed controller under a three-line-to-ground (3LG) with 45% voltage sag at the MV side is shown in Fig. 20. As the PI controller (PI-1) is tuned to be slow in order to track the MPP during normal operation, the parameters of this controller (PI-1) can be increased during the voltage sag in order to improve the performance of the proposed method.

Selected results on the performance of the system under different voltage sags and different solar radiation conditions are shown in Fig. 21. As demonstrated, the output currents always remain balanced during various types of faults and solar radiations and the dynamic performance of the proposed method to reach the new operating point is considerably fast. It should be mentioned that the ripples in the dc-link voltage in Fig. 21(f) and (h) are due to the unbalanced voltage sag.

The preference of the third method, i.e., injecting less power from the PV panels, compared to the first two methods is first due to its capability to inject active power into the grid during the voltage sag to support the grid. Second, it has the capacity to inject balanced currents into the grid even under unbalanced voltage conditions. The reason is the fact that the estimated active current reference given to the current limiter is obtained based on (15), which provides an almost constant value.

V. Conclusion

Performance requirements of GCPPPs under fault conditions for single- and two-stage grid-connected inverters have been addressed in this paper. Some modifications have been proposed for controllers to make the GCPPP ride-through compatible to any type of faults according to the GCs. These modifications include applying current limiters and controlling the dc-link voltage by different methods. It is concluded that for the single-stage configuration, the dc-link voltage is naturally limited and therefore, the GCPPP is self-protected, whereas in the two-stage configuration it is not. Three methods have been proposed for the two-stage configuration to make the GCPPP able to withstand any type of faults according to the GCs without being disconnected. The first two methods are based on not generating any power from the PV arrays during the voltage sags, whereas the third method changes the power point of the PV arrays to inject less power into the grid compared with the

prefault condition. The validity of all the proposed methods to ride-through voltage sags has been demonstrated by multiple case studies performed by simulations.

REFERENCES

[1] L. Trilla *et al.*, "Modeling and validation of DFIG 3-MW wind turbine using field test data of balanced and unbalanced voltage sags," *IEEE Trans. Sustain. Energy*, vol. 2, no. 4, pp. 509–519, Oct. 2011.

[2] M. Popat, B. Wu, and N. Zargari, "Fault ride-through capability of cascaded current-source converter-based offshore wind farm," *IEEE Trans. Sustain. Energy*, vol. 4, no. 2, pp. 314–323, Apr. 2013.

[3] A. Marinopoulos *et al.*, "Grid integration aspects of large solar PV installations: LVRT capability and reactive power/voltage support requirements," in *Proc. IEEE Trondheim PowerTech*, Jun. 2011, pp. 1–8.

[4] G. Islam, A. Al-Durra, S. M. Muyeen, and J. Tamura, "Low voltage ride through capability enhancement of grid connected large scale photovoltaic system," in *Proc. 37th Annu. Conf. IEEE Ind. Electron. Soc. (IECON)*, Nov. 2011, pp. 884–889.

[5] P. Dash and M. Kazerani, "Dynamic modeling and performance analysis of a grid-connected current-source inverter-based photovoltaic system," *IEEE Trans. Sustain. Energy*, vol. 2, no. 4, pp. 443–450, Oct. 2011.

[6] A. Yazdani *et al.*, "Modeling guidelines and a benchmark for power system simulation studies of three-phase single-stage photovoltaic systems," *IEEE Trans. Power Del.*, vol. 26, no. 2, pp. 1247–1264, Apr. 2011.

[7] A. Radwan and Y.-R. Mohamed, "Analysis and active suppression of ac- and dc-side instabilities in grid-connected current-source converter-based photovoltaic system," *IEEE Trans. Sustain. Energy*, vol. 4, no. 3, pp. 630–642, Jul. 2013.

[8] J. Miret, M. Castilla, A. Camacho, L. Garcia de Vicuna, and J. Matas, "Control scheme for photovoltaic three-phase inverters to minimize peak currents during unbalanced grid-voltage sags," *IEEE Trans. Power Electron.*, vol. 27, no. 10, pp. 4262–4271, Oct. 2012.

[9] G. Azevedo, P. Rodriguez, M. Cavalcanti, G. Vazquez, and F. Neves, "New control strategy to allow the photovoltaic systems operation under grid faults," in *Proc. Brazilian Power Electron. Conf. (COBEP)*, Sep. 2009, pp. 196–201.

[10] M. Mirhosseini, J. Pou, B. Karanayil, and V. G. Agelidis, "Positive- and negative-sequence control of grid-connected photovoltaic systems under unbalanced voltage conditions," in *Proc. Australasian Univ. Power Eng. Conf. (AUPEC)*, Sep. 2013, pp. 1–6.

[11] H. Seo, C. Kim, Y. M. Yoon, and C. Jung, "Dynamics of grid-connected photovoltaic system at fault conditions," in *Proc. Transmiss. Distrib. Conf. Expo. Asia Pacific*, Oct. 2009, pp. 1–4.

[12] A. Leon, J. Mauricio, and J. Solsona, "Fault ride-through enhancement of DFIG-based wind generation considering unbalanced and distorted conditions," *IEEE Trans. Energy Convers.*, vol. 27, no. 3, pp. 775–783, Sep. 2012.

[13] D. Campos-Gaona, E. Moreno-Goytia, and O. Anaya-Lara, "Fault ride-through improvement of DFIG-WT by integrating a two-degrees-of-freedom internal model control, in "*Proc. IEEE Trans. Ind. Electron.*, vol. 60, no. 3, pp. 1133–1145, Mar. 2013.

[14] G. Pannell, B. Zahawi, D. Atkinson, and P. Missailidis, "Evaluation of the performance of a dc-link brake chopper as a DFIG low-voltage fault-ride-through device," *IEEE Trans. Energy Convers.*, vol. 28, no. 3, pp. 535–542, Sep. 2013.

[15] B. Silva, C. Moreira, H. Leite, and J. Lopes, "Control strategies for ac fault ride through in multiterminal HVDC grids," *IEEE Trans. Power Del.*, vol. 29, no. 1, pp. 395–405, Feb. 2014.

[16] I. Erlich, C. Feltes, and F. Shewarega, "Enhanced voltage drop control by VSC; HVDC systems for improving wind farm fault ridethrough capability," *IEEE Trans. Power Del.*, vol. 29, no. 1, pp. 378–385, Feb. 2014.

[17] C. Feltes, H. Wrede, F. Koch, and I. Erlich, "Enhanced fault ride-through method for wind farms connected to the grid through VSC-based HVDC transmission," *IEEE Trans. Power Syst.*, vol. 24, no. 3, pp. 1537–1546, Aug. 2009.

[18] M. Mirhosseini, J. Pou, and V. G. Agelidis, "Single-stage inverter-based grid-connected photovoltaic power plant with ride-through capability over different types of grid faults," in *Proc. Annu. Conf. IEEE Ind. Electron. Soc. (IECON)*, Nov. 2013, pp. 8008–8013.

[19] M. Mirhosseini, J. Pou, and V. G. Agelidis, "Current improvement of a grid-connected photovoltaic system under unbalanced voltage conditions," in *Proc. IEEE ECCE Asia Downunder (ECCE Asia)*, Jun. 2013, pp. 66–72.

[20] E. Troester, "New german grid codes for connecting PV systems to the medium voltage power grid," in *Proc. 2nd Int. Workshop Conc. Photovoltaic Power Plants Opt. Des. Product., Grid Connect.*, Mar. 2009, pp. 1–4.

[21] BDEW. (2008, Jun.). *Technical Guideline-Generating Plants Connected to the Medium-Voltage Network- Guideline for Generating Plants Connection to and Parallel Operation with the Medium-Voltage Network* [Online]. Available: http://www.bdew.de/internet.nsf/id/A2A0475F2FAE8F44C12578300047C92F/$file/BDEW_RL_EA-am-MS-Netz_engl.pdf.

[22] SMA Solar Technology. (2013, Dec.). *Sunny Central 1000mv/1250mv/1600mv for Direct Medium-Voltage Feed-in* [Online]. Available: http://www.sma.de/en/products/central-inverters/sunny-central-1000mv-1250mv-1600mv.html

[23] SUNTECH POWER. (2013, Dec.). *295 Watt Polycrystalline Solar Module* [Online]. Available: http://www.suntech-power.com/en/products/utility-scale

[24] M. Mirhosseini and V. G. Agelidis, "Performance of large-scale grid-connected photovoltaic system under various fault conditions," in *Proc. IEEE Int. Conf. Ind. Technol. (ICIT)*, Feb. 2013, pp. 1775–1780.

[25] L. Shi and M. L. Crow, "Adaptive quadrant filter based phase locked loop system," in *Proc. North Amer. Power Symp. (NAPS)*, Sep. 2010, pp. 1–7.

[26] W. Yuan, W. Merk, H. Stemmler, and J. Allmeling, "Stationary-frame generalized integrators for current control of active power filters with zero steady-state error for current harmonics of concern under unbalanced and distorted operating conditions," *IEEE Trans. Ind. Appl.*, vol. 38, no. 2, pp. 523–532, Mar. 2002.

[27] S. Chung, "A phase tracking system for three phase utility interface inverters," *IEEE Trans. Power Electron.*, vol. 15, no. 3, pp. 431–438, May 2000.

[28] E. Robles *et al.*, "Variable-frequency grid-sequence detector based on a quasi-ideal low-pass filter stage and a phase-locked loop," *IEEE Trans. Power Electron.*, vol. 25, no. 10, pp. 2552–2563, Oct. 2010.

[29] T. Sezi, "Fast and accurate measurement of power system frequency," in *Proc. IEEE Power Energy Soc. Gen. Meeting*, Jul. 2010, pp. 1–7.

[30] J. Espina, A. Arias, J. Balcells, and C. Ortega, "Speed anti-windup PI strategies review for field oriented control of permanent magnet synchronous machines," in *Proc. Compat. Power Electron. (CPE)*, May. 2009, pp. 279–285.

[31] R. Teodorescu, M. Liserre, P. Rodriguez, and F. Blaabjerg, *Grid Converters for Photovoltaic and Wind Power Systems*. Hoboken, NJ, USA: Wiley, Jun. 2011.

Mitra Mirhosseini (S'13) received the B.Sc. and M.Sc. degrees in electrical engineering from Shahid Bahonar University of Kerman, Kerman, Iran, in 2007 and 2010, respectively. She is currently pursuing the Ph.D. degree at the School of Electrical Engineering and Telecommunications and the Australian Energy Research Institute (AERI), University of New South Walse (UNSW), Sydney, Australia.

Her research interests include modeling, control and performance of large-scale grid-connected photovoltaic power plants.

Josep Pou (S'97–M'03–SM'13) received the B.S., M.S., and Ph.D. degrees in electrical engineering from the Technical University of Catalonia (UPC), Catalonia, Spain, in 1989, 1996, and 2002, respectively.

In 1989, he was the Technical Director of Polylux S.A., Spain. In 1990, he joined the Faculty of UPC as an Assistant Professor, where he became an Associate Professor in 1993. Since February 2013, he has been a Professor with the University of New South Wales (UNSW), Sydney, Australia, on a leave from the UPC, where he keeps a permanent position. From February 2001 to January 2002 and from February 2005 to January 2006, he was a Researcher with the Center for Power Electronics Systems, Virginia Polytechnic Institute, State University (Virginia Tech), Blacksburg, VA, USA. From January 2012 to January 2013, he was a Researcher with the Australian Energy Research Institute (AERI), UNSW. He has authored more than 170 published technical papers and has been involved in several industrial projects and educational programs in the fields of power electronics and systems. His research interests include modeling and control of power converters, multilevel converters, renewable energy generation, and HVDC transmission systems.

Vassilios G. Agelidis (S'89–M'91–SM'00) was born in Serres, Greece. He received the B.Eng. degree in electrical engineering from Democritus University of Thrace, Thrace, Greece, in 1988, the M.S. degree in applied science from Concordia University, Montreal, QC, Canada, in 1992, and the Ph.D. degree in electrical engineering from Curtin University, Perth, WA, Australia, in 1997.

From 1993 to 1999, he was with the School of Electrical and Computer Engineering, Curtin University. In 2000, he joined the University of Glasgow, Glasgow, U.K., as a Research Manager for the Glasgow-Strathclyde Centre for Economic Renewable Power Delivery. In addition, he has authored/coauthored several journal and conference papers as well as *Power Electronic Control in Electrical Systems* in 2002. From January 2005 to December 2006, he was the inaugural Chair of Power Engineering with the School of Electrical, Energy and Process Engineering, Murdoch University, Perth. From December 2006 to June 2010, he was the Energy Australia Chair of Power Engineering with the University of Sydney, Sydney, Australia. He is currently the Director of the Australian Energy Research Institute, University of New South Wales (UNSW Australia), Sydney, Australia.

Dr. Agelidis received the Advanced Research Fellowship from the United Kingdom's Engineering and Physical Sciences Research Council in 2004. He was the Vice President Operations within the IEEE Power Electronics Society from 2006 to 2007. He was an Associate Editor of the IEEE POWER ELECTRONICS LETTERS from 2003 to 2005, and served as the Power Electronics Society (PELS) Chapter Development Committee Chair from 2003 to 2005. He was an AdCom Member of IEEE PELS from 2007 to 2009 and the Technical Chair of the 39th IEEE Annual Power Electronics Specialists Conference, Rhodes, Greece.